Asian Journal of Chemistry Vol. 17, No. 2 (2005), 1078–1092

Chemical and Structural Properties of Jordanian Diatomaceous Clay Supported Metal Oxides

SALEM M. MUSLEH
Department of Chemistry, Faculty of Science and Information Technology, Al-Balqa Applied University, Al-Salt 19117, Jordan
E-mail: smusleh@lycos.com

Metal oxides of titanium and vanadium were deposited on the native Jordanian diatomaceous clay. The chemical and structural properties of the prepared samples were investigated using XRF, ICP, XRD and FTIR techniques. The diatomaceous clay supported metal oxides were used in preliminary experiments to explore their interaction with aqueous phenol solution under thermal and photochemical conditions, in the presence and absence of hydrogen peroxide. The results showed that the metal oxides have interacted with diatomaceous clay and caused some structural changes. These were reflected in the surface area of the samples and their activity in the phenol reactions.

Key Words: Diatomaceous clay, Titanium oxides, Vanadium pentoxide, Phenol, Adsorption.

INTRODUCTION

Jordanian diatomaceous deposits were first discovered in 1990, at Al-Azraq region, 110 km east of Amman, within an area of about 150 km^2. It is found naturally mixed with clays, so it is called diatomaceous clay. The chemical composition of Jordanian diatomaceous clay, which has a moderate silica content, about 74%, and relatively high amounts of alumina and iron-oxide, 10 and 5.2%, respectively, is comparable with that of other regions, particularly with the Moler from Denmark. In Al-Azraq region, the predominant diatoms were monospecies of discoid or cylindrical shapes[1].

The unique combination of physical and chemical properties of diatomite makes it suitable for a wide range of important applications[2-4]. Among such applications is its use as a support for transition metal oxides[5] and oxidation catalyst for the removal of nitrogen oxides from waste gases[6].

The purpose of the present work is to explore, through thermal treatment and chemical deposition of metal oxides, to impart some useful properties to the native Jordanian diatomaceous clays and to investigate, after characterization of the products, their possible use in the removal of organic pollutants from contaminated waters. Towards this end, samples of native diatomaceous clays were selected to have a silica content that falls near the average for Al-Azraq deposits, which ranges between 41–76%.

Phenols, from both industrial or agricultural sources, are major pollutants in some of the waters in Jordan. It was, therefore, decided to study the use of diatomaceous clay supported metal oxides for the removal of phenols from aqueous media. The oxides, *i.e.*, titanium oxides, both rutile, anatase and vanadium pentoxide, chosen for this purpose were known for their activity in this respect. The preparation and characterization of these modified clays are reported, together with preliminary results of their possible use for the removal of phenol from aqueous solution.

EXPERIMENTAL

Diatomaceous clays were supplied by the Jordanian Natural Resources Authority (JNRA) and samples were chosen to have the near average silica content, which were then homogenized and their chemical composition was ascertained by XRF analysis. These samples were labelled D.

Quantities of D were cleaned by successive washings with distilled water, then with a solution consisting of tetrasodium pyrophosphate (0.05 M) and sodium hydroxide (0.05 M) (1 : 1 ratio), followed by washing with sodium hydroxide solution (0.05 M) and finally with distilled water[7]. The samples were dried overnight in an oven at 100°C. Particles larger than 250 μm were removed by mechanical sieving. The cleaned samples were labelled C.

To investigate the effect of calcination, a 10 g of sample C was heated in a muffle furnace to 500°C for 12 h. The chemical composition and mineral constitution of the calcined diatomaceous clay, referred to as sample C_0, were then used for comparison with similarly treated samples after deposition of the metal oxides.

Metal oxide deposition: The oxides of titanium and vanadium were deposited from solutions of their appropriate salts on the diatomaceous clay, following the procedure outlined below.

Deposition of titanium oxides: The deposition of the titanium oxides on diatomaceous clay was affected *in situ* by the hydrolysis of titanium tetrachloride for the rutile form and titanium(IV) sulfate for the anatase form[8]. Thus, 10 g sample of C was suspended in water and the corresponding titanium reagent was added gradually with stirring. The mixture was then neutralized with ammonia solution; after 2 h it was filtered and the product was dried at 100°C, followed by calcination for 12–16 h in a muffle furnace at 250°C for the rutile sample C-11 and 500°C for the anatase sample C-12.

The results of ICP analysis for the percentage of TiO_2 in the samples gave for C-11 34.41% and for C-12 11.28%.

For the purpose of comparison, rutile and anatase samples were prepared by similar procedures, but in the absence of diatomaceous clay. The products TiO_2 (anatase) and TiO_2 (rutile) were identified by powder XRD and KBr-matrix FTIR[9, 10]. The C-11 and C-12 samples were also shown by the same techniques to carry rutile and anatase, respectively.

Deposition of vanadium pentoxide: Vanadium pentoxide was deposited on diatomaceous clay by *in situ* hydrolysis of ammonium metavanadate.

Two methods were used. In the first, for samples C-21 and C-22, the hydrolysis was affected by the use of sulfuric acid, following the method described by Lee[11]. The product was thoroughly washed with water, dried and calcined at 500°C for 12 h. In the preparation of C-22, the supported V_2O_5 was further washed with ammonical solution and after thorough washing with water, it was further calcined at 500°C for 12 h.

In the second method, for sample C-23, the hydrolysis was carried out using 0.3 M ammonia solution, according to the procedure described by Eiji *et al.*[12] Again after washing and drying, the sample was calcined at 500°C for 12 h, then washed with water and again calcined at 500°C for 12 h.

The results of ICP analysis gave the percentage of vanadium pentoxide in the samples as 14.01, 10.98 and 1.61% for C-21, C-22 and C-23, respectively.

For comparison, a sample of V_2O_5 was also prepared by the method described by Lee[11]. The power XRD patterns and the KBr-matrix FTIR spectra were used for characterization. Comparison of the XRD patterns for the samples with those of diatomaceous clay sample C_0 and solid V_2O_5 was inconclusive. However, the IR spectra, in the region of the characterization bands for V_2O_5, showed the distinct presence of the oxide in diatomaceous clay samples[13].

Characterization of materials

All samples were characterized by ascertaining their chemical composition, mineral constitution and chemical bonding as well as their surface morphology and adsorption capacity.

The chemical composition was determined using XRF and ICP techniques, at Natural Resources Authority (NRA), Amman, Jordan. The instruments used were Diano model 2023 and ARL model 3410 ICP, respectively. The operating conditions were followed as presented by the manufacturers. For XRF measurements, 0.8 g of the sample was thoroughly mixed with 7.2 g of lithium tetraborate in a platinum crucible, which was introduced into an automatic fluxer, LECO Corp. model FX-200, where a temperature program was affected starting from room temperature to 1200°C. The melt was then poured into a casting dish and allowed to cool. The resultant glassy disc was used for XRF analysis. In the ICP technique, the sample was well ground to pass a 100 mesh sieve, then mixed with sodium peroxide and heated to 450°C for 45 min in a Zr-crucible. The residue was treated with hydrochloric acid and filtered. The filtrate was then introduced into the analyzer to a flow rate of 3 mL/min.

The mineral constitution of the samples was determined at NRA by powder XRD technique, using Rigaku UK 10392 diffractometer fitted with Philips X-ray tube giving CuK_α radiation (λ = 1.5418 Å), at 40 kV and 40 mA.

The chemical constitution of the samples was investigated by FTIR technique using KBr-matrix. The instrument was Nicolet Impact model 400 FTIR spectrometer and the scanning range was 4000–400 cm^{-1}. All samples were thoroughly ground with dried KBr using agate mortar and pestle. Transparent discs were obtained using hydraulic press at 12 ton/m^2.

Surface area estimation

The surface areas of samples were estimated using the methylene blue method, which was known to give good estimates of surface areas for siliceous materials[15–17].

Weight samples of solids were left at room temperature in contact with carefully prepared aqueous solutions of methylene blue for four weeks in subdued light to reach equilibirum. The methylene blue concentration was determined spectrophotometric at λ 602 nm.

Interaction with aqueous phenol

To investigate the interaction of aqueous phenol with the prepared samples, two experiments were conducted. In the first, the interaction was carried out at a constant temperature of 53 ± 1°C in the presence of hydrogen peroxide, using 150 mL aqueous solution containing 5000 ppm phenol.

In the second set, a photochemical reactor fitted with high pressure Hg-lamp, Haraeus model Hpk-125 was used. The reaction was carried out in the presence and absence of hydrogen peroxide. For the former, phenol solution of 5000 ppm was used, while for the latter, a solution containing 100 ppm phenol was used. The reactions in both, the thermal and photochemical, experiments were followed by phenol derivatization with 4-aminoantipyrine, in buffered basic medium (pH 9), according to the method described by Blo *et al.*[18] The concentration of derivatized phenol was determined spectrophotometrically at λ 455 nm.

RESULTS AND DISCUSSION

The chemical composition of all the samples as determined by XRF and ICP techniques are shown in Tables 1 and 2, respectively. These results will be discussed in terms of the change in the relative presence of the main constituents, *viz.*, Al_2O_3, SiO_2, Fe_2O_3, MgO, CaO, K_2O and Na_2O, expressed as ratios to the major constituent SiO_2. These ratios, which are referred to as indicator ratios, are given in Tables 3–5.

TABLE-1
THE XRF ANALYSIS OF SAMPLES EXPRESSED AS WEIGHT PER CENT OF OXIDES

Code	SiO_2	Al_2O_3	TiO_2	MnO	Fe_2O_3	MgO	CaO	K_2O	Na_2O	P_2O_5	Total
D	52.38	13.91	0.89	0.10	7.30	2.79	3.85	2.53	0.970	0.170	84.89
C_0	53.46	12.78	0.85	0.06	6.62	2.93	5.12	2.82	0.190	0.140	85.07

The main effect of the raw material treatment, as shown by the indicator ratios given in Table-3, is the marked decrease in the sodium content and the marked increase in the calcium content. The treatment seems to have also moved the MgO/CaO ratio to that obtained in dolomite (*i.e.*, 0.72).

TABLE-2
THE ICP ANALYSIS EXPRESSED AS WEIGHT PER CENT OF OXIDES

Code	SiO_2	Al_2O_3	TiO_2	MnO	Fe_2O_3	V_2O_5	MgO	CaO	K_2O	P_2O_5	Total
C_0	47.14	13.06	00.93	0.06	6.25	0.027	2.76	3.22	2.47	0.29	77.26
C-11	23.85	06.98	34.41	0.03	3.17	0.012	1.22	1.51	1.18	0.15	72.51
C-12	48.92	13.23	11.28	0.01	3.87	0.021	0.07	0.16	1.99	0.13	79.68
C-21	51.96	12.45	1.020	0.02	5.31	14.01	1.14	0.73	2.44	0.12	89.20
C-22	52.36	12.12	0.990	0.02	4.87	10.98	1.06	1.26	2.33	0.13	86.12
C-23	61.12	13.38	1.140	0.07	6.63	1.610	2.93	4.12	3.16	0.28	94.44

TABLE-3
INDICATOR RATIOS FOR SAMPLES D AND C_0

Ratios	D	C_0
Al_2O_3/SiO_2	0.270	0.240
Fe_2O_3/SiO_2	0.140	0.120
Fe_2O_3/Al_2O_3	0.520	0.520
MgO/SiO_2	0.053	0.055
CaO/SiO_2	0.074	0.098
MgO/CaO	0.720	0.560
K_2O/SiO_2	0.048	0.053
Na_2O/SiO_2	0.018	0.004
Na_2O/K_2O	0.380	0.067

The titanium samples show clearly the effect of the sample preparation procedure on their composition. Thus, in sample C-12, where the general effect of the strong acid environment (*i.e.*, H_2SO_4) decreases uniformly in the presence of all constituents relative to silica as shown in Table-4.

TABLE-4
INDICATOR RATIOS FOR SAMPLES C_0, C-11 and C-12

Ratios	C_0	C-11	C-12
TiO_2/SiO_2	2.040	144.300	23.060
Al_2O_3/SiO_2	0.280	0.290	0.270
Fe_2O_3/SiO_2	0.130	0.130	0.080
Fe_2O_3/Al_2O_3	0.480	0.450	0.290
MgO/SiO_2	0.059	0.051	0.015
CaO/SiO_2	0.068	0.063	0.003
MgO/CaO	0.860	0.810	0.440
K_2O/SiO_2	0.052	0.050	0.041

The indicator ratios for the vanadium oxide samples (Table-5) show a general decrease in the Al_2O_3/SiO_2 ratio. However, the MgO/CaO ratio fluctuated and in sample C-23 was the closest to that for dolomite, which fact is supported by the appearance of the dolomite characteristic peak in the XRD pattern of that sample.

TABLE-5
INDICATOR RATIOS FOR SAMPLES C_0, C-21, C-22 and C-23

Ratios	C_0	C-21	C-22	C-23
V_2O_5/SiO_2	0.060	26.960	20.970	2.630
Al_2O_3/SiO_2	0.280	0.240	0.230	0.220
Fe_2O_3/SiO_2	0.130	0.100	0.009	0.110
Fe_2O_3/Al_2O_3	0.480	0.430	0.400	0.500
MgO/SiO_2	0.059	0.022	0.020	0.048
CaO/SiO_2	0.068	0.014	0.024	0.067
MgO/CaO	0.860	1.600	0.850	0.710
K_2O/SiO_2	0.052	0.047	0.044	0.052

Mineral constitution

The XRD patterns support the notion that the native Jordanian diatomaceous samples are best referred to as diatomaceous clay. Thus, beside the presence of the amorphous opal as the main component in diatomite, that of crystalline constitutions is quite evident, as shown by the results presented in Table-6.

TABLE-6
MINERAL CONTENTS OF DIATOMACEOUS CLAY SAMPLES

Mineral type	D	C_0	C-11	C-12	C-21	C-22	C-23
Quartz	XX	XXX	XXX	XXX	XXX	XXX	XXX
Kaolinite	XX	X	X	—	—	—	—
Feldspar	X	X	—	—	XX	XXX	XX
Muscovite	X	XX	—	—	—	X	XX
Dolomite	—	XX	—	—	—	—	XX

XXX: Major; XX: Minor; X: Trace

In the case of the raw diatomaceous clay, D, XRD patterns (Fig. 1) indicate the presence of quartz but less significantly than in the treated sample, C_0: however, the total silica content for both was about 54% as given by XRF analysis (Table-1). This indicates that while SiO_2 is present mainly as amorphous opal in the untreated sample, D, quartz forms a major component in the treated diatomaceous clay, C_0.

This can be explained as due to the calcination process, since α-quartz is a stable mineral form of silica at 500°C. The conversion to quartz is also accompanied, as to be expected[19], by the formation of dolomite which was observed in the treated sample, C_0 (Fig. 1).

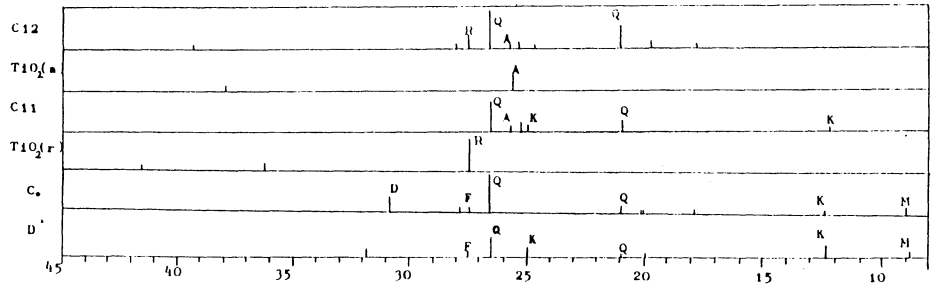

Fig. 1. X-ray diffraction patterns for Ti-oxide modified diatomaceous clays

Other minerals present in the raw sample, as minor traces, are feldspar and muscovite, with the latter increasing markedly in C_0. Kaolinite, however, seems to be very sensitive to calcination and the procedures followed in the sample preparation; thus it has become only a trace component.

The XRD data for Ti-oxides modified diatomaceous clay, C-11 and C-12, together with those of the prepared rutile and anatase are compared (Fig. 7), from which the presence of rutile and anatase in C-11 and C-12 could be surmised. However, while TiO_2 in C-11 seemed to be of the anatase form, that in C-12 gave an indication of the presence of anatase as well as rutile.

TABLE-7
MAJOR ABSORPTION BANDS OF THE DIATOMACEOUS CLAY SAMPLES IN THE 1000 cm^{-1} REGION

Code	Major absorption bands (cm^{-1})
D	1038
C_0	1043
C-11	988, 1032, 1093
C-12	1047
C-21	1029, 1051
C-22	1060
C-23	1043

In the preparation of C-11, it was expected that the hydrolysis of $TiCl_4$ would give the rutile form of TiO_2 deposited on the diatomaceous clay. However, the peak at $2\theta = 25.6°$ indicates clearly that the oxide was deposited in the anatase form. The formation line at $2\theta = 25.2°$ is common between C-11 and C-12, indicating the formation a common form of titanium containing mineral in these two samples.

Quartz content remained high in C-12, but somewhat decreased in C-11. Kaolinite disappeared in C-12 but it was only a trace in C-11. On the other hand, feldspar and muscovite both disappeared in C-11 and C-12. All of these changes may be due to differences in samples preparation procedure. In C-12, sulfuric acid was used, while in the preparation of C-11, hydrochloric acid was produced

which may have affected the mineralogy of the samples. The absence of dolomite could also be attributed to the presence of these strong acids.

In C-21, C-22 and C-23, presence of V_2O_5 in the samples could not be conclusively ascertained from XRD patterns. However, the peaks in the $2\theta = 25.5°$ region for all samples, and at $2\theta = 36.6°$ in C-21 and C-23, have no counterpart in C_0 (Fig. 2).

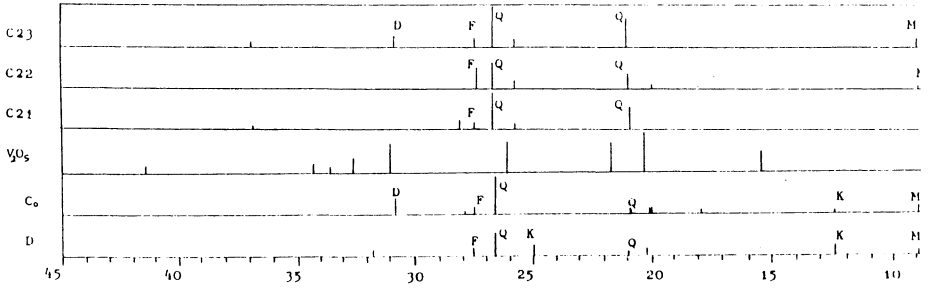

Fig. 2. X-ray diffraction patterns for V_2O_5 modified diatomaceous clays

Quartz remained as a major component in C-21 and C-23, but somewhat unexpectedly decreased in C-22. This may be due to washing with dilute ammonia. Kaolinite disappeared from the three samples. Muscovite appeared as trace in C-22, but increased only slightly in C-21 and C-23. Dolomite was almost removed in C-21 and C-22, since their preparation involved the use of sulfuric acid, but in C-23 dolomite presence was quite evident.

In spite of the presence of the added metal oxides as evidenced by the XRF and ICP analysis results, the rather inconclusiveness of the XRD patterns, for some of the samples, could be explained as either that the metal oxides deposited mainly in amorphous forms or that the hydrolysis of the metal salts involved interaction with the substrates through interstitial substitution or by attachment to silicon or aluminium to form Si(Al)-O-M.

Chemical constitution

The infrared spectra of the samples further helped in their characterization. Thus, the spectrum of untreated diatomaceous clay, D (Fig. 3), shows the general characteristic bands of opal line silica as well as those of quartz[9, 20], and Kaolinite[21]

The bands due to kaolinite are well represented specially in the 1200–950 and 4000–3000 cm^{-1} regions. The expected quartz doublet at 790–780 cm^{-1} is not clearly evident in the spectrum possibly due to the overlap with the kaolinite band in the same region. However, the peaks at 1972, 463 and 522 cm^{-1} which are unexpectedly quite sharp, may be due to the diatomite in the sample.

The spectrum of the washed and calcined sample C ideally shows the main changes that have occurred. Thus, the appearance of the doublet at 776 and 798 cm^{-1} is strong evidence for the presence of quartz. The broadening of the bands at 560–400 and 1200–900 cm^{-1} reflects the overlap of strong bands of the main minerals present, which are indicated by XRD result, *viz.*, quartz, dolomite and muscovite.

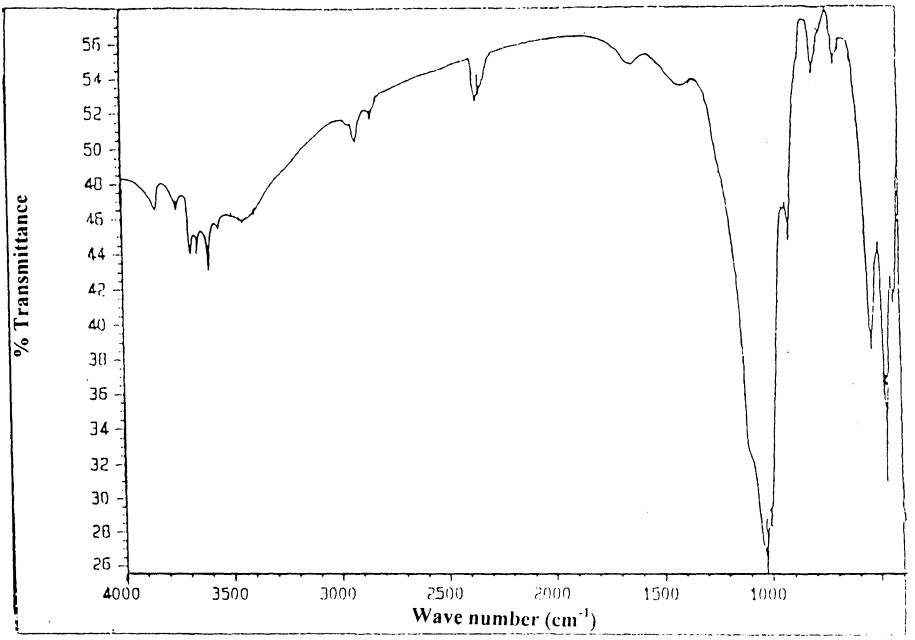

Fig. 3. FTIR spectrum of sample D in the range 4000–400 cm^{-1}

The presence of water, whether free or combined, as well as the Si(Al)—OH groups, is shown by the bands in the region 4000–3500 cm^{-1} and illustrated in Fig. 4. This is of practical interest because, as to be expected, changes in this region would indicate the possible effect of the added metal oxides.

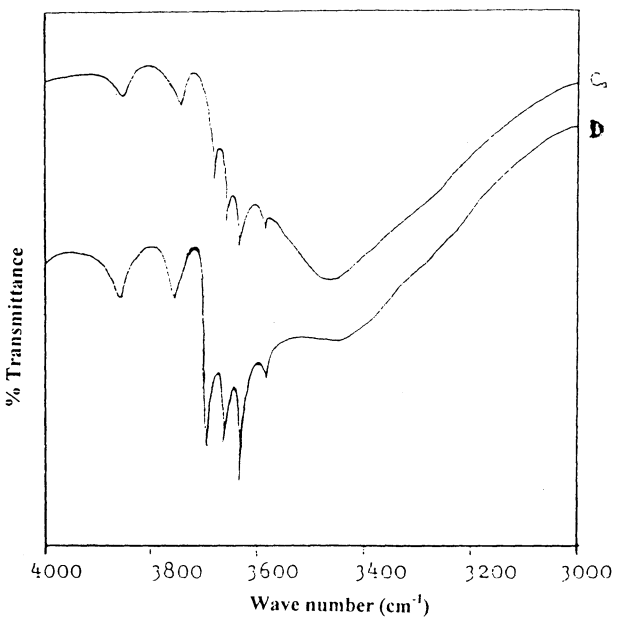

Fig. 4. FTIR spectra of C_0 and D in the range 4000–3000 cm^{-1}

The presence of metal oxides in the diatomaceous clay samp'es is evidenced by some marked changes in their spectra as compared to that of the reference sample C_0. These changes are marked in the spectral regions 4000–3000 and 1500–700 cm^{-1} respectively (Figs. 5 and 6).

In the Ti-oxide sample C-11, the quartz doublet at 800–780 cm^{-1} is not clearly shown, while in the spectrum of sample C-12, the doublet is quite evident. The shift in the strong peak appearing in the 1000 cm^{-1} region, as well as the changes in the 4000–3000 cm^{-1} region (Figs. 5 and 6), all point to the possible formation of Si—O—Ti linkage for both samples.

The most significant changes observed in the spectra of the vanadium oxide samples C-21, C-22 and C-23, is the shift in the strong band in the 1000 cm^{-1} region and again, the changes in the 4000–3000 cm^{-1} region. However, in all these samples, quartz doublet has persisted.

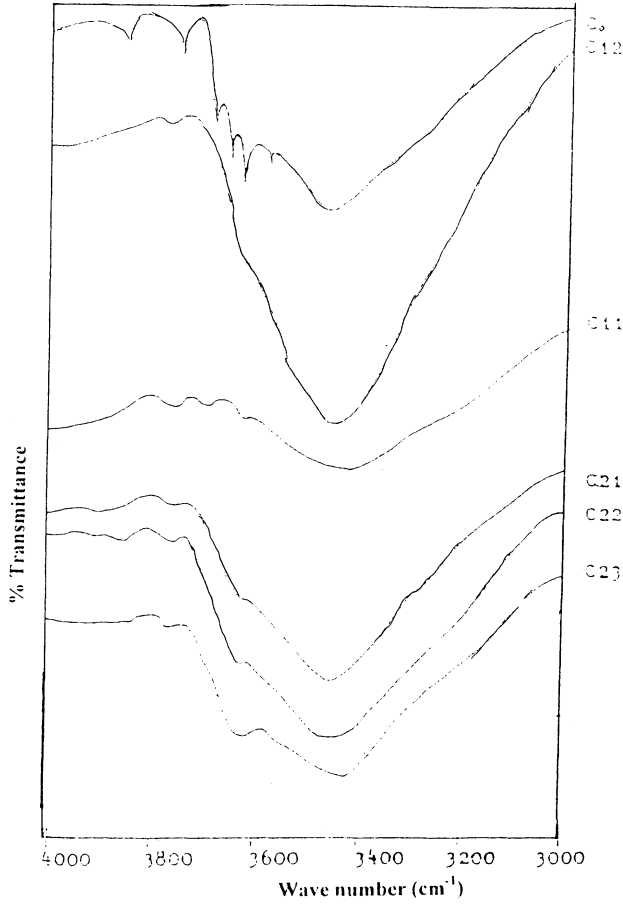

Fig. 5. FTIR spectra of diatomaceous clay samples in the region 4000–3000 cm^{-1}

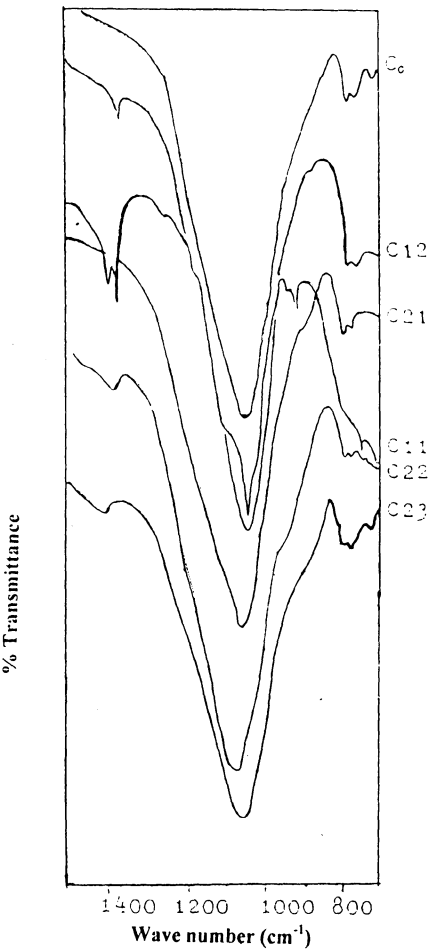

Fig. 6. FTIR spectra of diatomaceous clay samples in the region 1500–700 cm^{-1}

The presence of dolomite is not as well evidenced as would have been expected from the XRD results for samples C_0, C-23 and C-31. However, the bands at 727 and 1400 cm^{-1} can very well be attributed to the presence of dolomite in the above samples.

In general, the changes observed in the spectra of metal oxides modified diatomaceous clay samples all indicate the possible formation of Si—O—M linkages. This is manifested by the contours and shifts in the Si—O—Si band in the 1000 cm^{-1} region (Fig. 6 and Table-7).

Surface areas: The methylene blue adsorption method was used to obtain estimated surface areas of all the samples, from which relative values were obtained for comparison, as summarized in Table-8.

For the diatomaceous clay modified with TiO_2, sample C-12 the measured relative surface areas showed a significant increase compared with the treated diatomite C_0. On the other hand, C-11 gave nearly the same surface area as C_0, while C-22 gave relative surface areas slightly lower than that of C_0. Furthermore,

the results obtained from samples C-21 failed to conform with Langmuir's adsorption isotherm.

It was observed that, with the exception of C-12 and C-42, as the deposited metal oxide decreased, relative surface area increased (Table-8). This may be interpreted by the fact that as metal oxide content increases, greater number of active sites (acidic positions) will be covered by the deposited metal oxide and the adsorption of methylene blue will decrease.

TABLE-8
SURFACE AREAS OF DIATOMACEOUS EARTH CLAY SAMPLES AND THEIR SILICA AND ALUMINA CONTENTS, DEPOSITED METAL OXIDE, b_2, b_1 RATIO CRYSTALLITE SIZE

Code	Clay	Estimated surface area (m^2/g)	Relative surface area	Relative crystallite size	b_2/b_1 ratio	SiO_2 (%)	Al_2O_3 (%)	Deposited metal oxide (%)
C_0	Treated clay	104	1.00	1.00	1.44	53.46	12.78	—
C-11	TiO_2/C	101	0.97	1.70	2.40	23.90	6.98	34.4
C-12	TiO_2/C	182	1.80	0.83	2.03	48.90	13.20	11.3
C-21	V_2O_5/C	—	—	1.20	1.82	52.00	12.40	14.0
C-22	V_2O_5/C	76	0.73	1.20	1.61	52.40	12.10	11.0
C-23	V_2O_5/C	81	0.78	1.10	1.37	61.1	13.40	1.61

b_2: Peak height of molecular H_2O (peak 3430 cm^{-1})
b_1: Peak height of the hydroxyl group (Si—OH). (Peak at 3620 cm^{-1}).

In general, the increase in the silica and alumina contents of samples is followed by an increase in the relative surface areas. This could be considered due to the preference of the methylene blue to be adsorbed on acidic sites.

The FTIR spectra and the data (Table-8), show that as the ratio between the height of the peak due to H_2O stretching vibration at 3430 cm^{-1} (b_2) to that of hydroxyl group (Si—OH) at 3620 cm^{-1} (b_1) increases, the relative surface area decreases. The increase in the height of the 3620 cm^{-1} is a good indication of the increased polarity of the surface and thus, leads to greater affinity for the polar methylene blue molecules.

Since quartz forms the main mineral type of all the treated diatomaceous clay samples, the broadening of the band of quartz in the XRD trace at $2\theta = 26.6$ may be taken as a good indication of change in crystallite size[22]. It is interesting to observe how this may correlate with the surface area of the samples. From the data (Table-8), it is clear that as the quartz relative crystallite size decreases, the relative surface area increases.

Reactions of aqueous phenol in the presence of clay supported metal oxides

Preliminary work was carried out to investigate the possible effect of the presence of the metal oxides supported on diatomaceous clays on phenol in aqueous medium under thermal and photochemical reaction conditions with and

without hydrogen peroxide. For this purpose, a selected number of samples were chosen for each oxide type and the reaction was followed over time (Figs. 7 and 8) and the initial rates were estimated (Table-9).

The data given in Table-9 and Fig. 7 show that the initial rate of the reaction

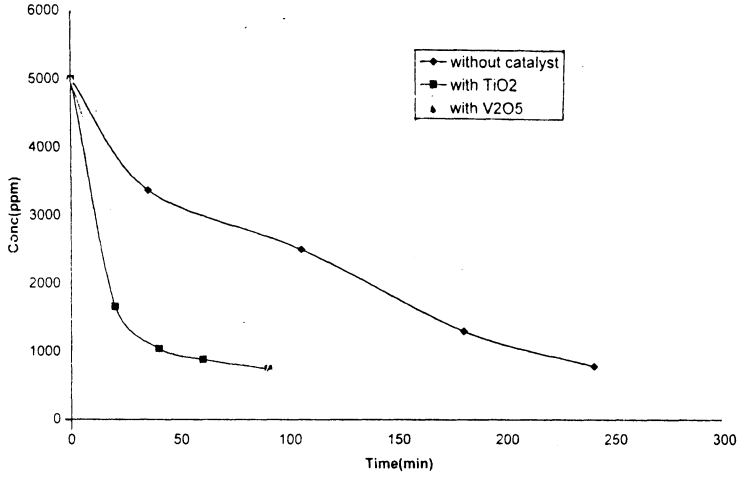

Fig. 7. The reaction of aqueous phenol thermally with hydrogen peroxide in the absence and presence of diatomaceous clay samples

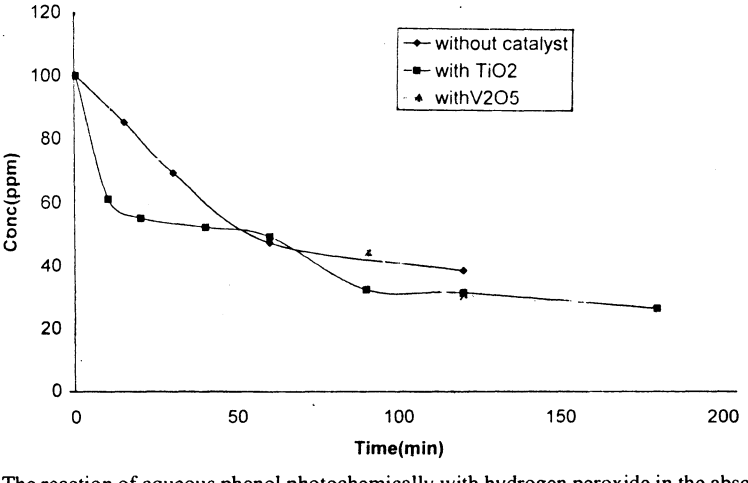

Fig. 8. The reaction of aqueous phenol photochemically with hydrogen peroxide in the absence and presence of diatomaceous clay samples

of phenol and hydrogen peroxide under thermal condition increased four times in the presence of treated clay C_0. A significant increase in the initial rate was also observed in the presence of the metal oxide modified samples. The increase in the initial reaction rates follows the sequence: C-22 > C-11 > C_0 > without clay.

TABLE-9
INITIAL RATE (v_0) OF THE REACTION OF AQUEOUS PHENOL UNDER DIFFERENT EXPERIMENTAL CONDITIONS

Code	Sample	Initial rate (v_0) (ppm/min) (H_2O_2 + heat)	Initial rate (v_0) (ppm/min) (UV + H_2O_2)	Initial rate (v_0) (ppm/min) (UV radiation)
	No clay	1.7	22	0.88
C_0	Treated clay	7.1	120	0.90
C-11	TiO_2/C	18	99	2.20
C-12	V_2O_5/C	27	88	0.57

It is interesting to note that the initial rates for clay sample C-22 are quite different compared with those for sample C-11. The higher rates observed for the manganese oxides and vanadium oxide may have been due to their greater oxidative power relative to iron and titanium oxides.

When phenol was irradiated with UV-light, in the absence of hydrogen peroxide, the following decreasing order of the initial reaction rates was observed (Fig. 8 and Table-9) (C-11 > C_0 ≈ without clay > C-22). The high reactivity in the presence of TiO_2 is quite evident.

In the presence of hydrogen peroxide, the initial rate increased significantly in the presence of treated clay (Table-9). The presence of metal oxides, however, showed no great effect. Nevertheless, the order of decrease in the initial rates of the photochemical reaction of phenol with hydrogen peroxide is as follows: C_0 > C-11 > C-22 > without clay.

The above trend generally followed the increase in the surface area of the clay samples. Sample C-11 gave the highest initial rate in comparison with the other metal oxide modified surfaces. This may be due to the fact that TiO_2 is a semiconductor, which can be activated, by UV-radiation, to produce surfacial holes which may then participate in the hydrogen peroxide reaction with phenol[23].

ACKNOWLEDGEMENT

Thanks are due to the Natural Resources Authority (Amman) for the use of their chemical analytical facilities.

REFERENCES

1. J. Allali and M. Qararah, Diatomite in Jordan, Basman Press, Amman, Jordan, pp. 47–48 (1995).
2. F.M. Herman, Enclyclopedia of Chemical Technology, Vol. 7, 2nd Edn., John Wiley & Sons, New York, pp. 603–614 (1972).
3. R.W. Fairbidge and D. Jablonski, Enclyclopedia of Paleontology, Dowen, Hutchinson & Ross, Strondsburgh, pp. 247–252 (1979).
4. S.D. Inglethorpe and D.J. Morgan, The Laboratory Assessment of Diatomite, National Conference on Geologic Resources of Thialand: Potential for Future Development, Department of Mineral Resources, Bangkok, Thailand, pp. 210–221 (1992).
5. O. Kyoji, S. Kenichi and Y. Takeshi, Eur. Pat. Appl. EP. 58, 046 (C1. C07C47/22). *Chem. Abstr.*, **98**, 107930d (1982).

6. W. Von Wedel, E.R. Barenschee and H. Eickhoff, Ger. DE 4, 136, 183 (Cl. BO1D53/36); *Chem. Abstr.*, **119**, 145653a (1993).
7. E.L. Poutanen and R.J. Moris, *Estuarine, Coastal Shelf Sci.*, **17**, 189 (1983).
8. M. Inomata, K. Morl, A. Ui, T. Miyamoto and M. Yuichi, *J. Phys. Chem.*, **87**, 754 (1983).
9. J.A. Gadsden, Infrared Spectra of Minerals and Related Inorganic Compounds, Butterworths, London, p. 277 (1975).
10. H.W. Van Der Marel and H. Beutelspacler, Atlas of Infrared Spectroscopy of Clay Minerals and Their Admixture, Elsevier, Amsterdam, pp. 276–280 (1976).
11. J.D. Lee, Concise Inorganic Chemistry, 2nd Edn., D. Van Nostrand, London, pp. 706–707 (1966).
12. I. Eiji, A. Ken-Ishi and O. Takaharu, *Bull. Chem. Soc. (Japan)*, **59**, 1665 (1986).
13. L.D. Frederickson and D.M. Hausen, *Anal. Chem.*, **44**, 1325 (1972).
14. S.J. Gregg and K.S.W. Sing, Adsorption, Surface Area and Porosity, Academic Press, London, pp. 65–70 (1967).
15. P.T. Hang and G.W. Brindley, *Clays Clay Miner.*, **18**, *203 (1970).*
16. B. Rossela and A. De Buttisti, *J. Chem. Edu.*, **64**, 175 (1987).
17. J.H. Potgieter, *J. Chem. Edu.*, **68**, 349 (1991).
18. G. Blo, F. Dondi and C. Bighi, *J. Chromatogr.*, **295**, 231 (1984).
19. W.A. Deer, R.A. Howie and J. Zussman, An Introduction to the Rock Forming Minerals, 2nd Edn., Longman Scientific and Technical, London, p. 696 (1992).
20. V.C. Farmer, The Infrared spectra of Minerals, Mineralogical Society, London, pp. 365–370 (1974).
21. M.J. Wilson, Clay Mineralogy: Spectroscopic and Chemical Determinative Methods, Chapman & Hall, London, pp. 11–64 (1994).
22. G.C. Bond, Heterogeneous Catalysis: Principles and Applications, 2nd Edn., Clarendon Press, Oxford, pp. 80–82 (1987).
23. P.D. Allen and C.B. Huang, *Water Res.*, **24**, 543 (1990).

(*Received*: 22 July 2004; *Accepted*: 3 January 2005) AJC-4051